Water vapor isotopes indicating rapid shift among multiple moisture sources for the 2018/2019 winter extreme precipitation events in Southeast China

Tao Xu[1], Hongxi Pang[1,2], Zhaojun Zhan[1], Wangbin Zhang[1], Huiwen Guo[1], Shuangye Wu[3], and Shugui Hou[1,4]

[1] Key Laboratory of Coast and Island Development of Ministry of Education, School of Geography and Ocean Science, Nanjing University, Nanjing, 210023, China

[2] Collaborative Innovation Center of Climate Change, Jiangsu Province, Nanjing, 210023, China

[3] Department of Geology and Environmental Geosciences, University of Dayton, Dayton, OH 45469, USA

[4] School of Oceanography, Shanghai Jiao Tong University, Shanghai, 200240, China

Correspondence: H. Pang (hxpang@nju.edu.cn) and S. Hou (shuguihou@sjtu.edu.cn)

Abstract. In the East Asian monsoon region, winter extreme precipitation events occasionally occur and bring great social and economic losses. From December 2018 to February 2019, Southeast China experienced a record-breaking number of extreme precipitation events. In this study, we analyzed the variation of water vapor isotopes and their controlling factors during the extreme precipitation events in Nanjing, Southeast China. The results show that the variations of water vapor isotopes are closely linked to the change of moisture sources. Using a water vapor d-excess weighted trajectory model, we identified five most important moisture source regions: South China, East China Sea, South China Sea, Bay of Bengal, and Continental regions (Northwest China and Mongolia). Moreover, the variations of water vapor d-excess during a precipitation event reflect rapid shifts of moisture source regions. These results indicate that rapid shifts among multiple moisture sources are important conditions for sustaining wintertime extreme precipitation events over extended periods.

1 Introduction

South China is under the influenced of the East Asian Winter Monsoon during winter with prevailing northeasterly wind. As a result, winter precipitation is significantly less than summer (Yao et al., 2015), accounting for approximately 10% of the

total annual precipitation (Wang and Feng, 2011). However, persistent extreme winter precipitation events still occur occasionally (Huang et al., 2018a; Li et al., 2020a), such as the disastrous snowstorm in January 2008 (Ding et al., 2008), which caused great losses in agriculture, transportation, and electric power facilities (Zhou et al., 2011). Such extreme events are likely to become more frequent with global warming (Rahmostorf and Coumou, 2011; Qin et al., 2021). Therefore, improving the understanding of the characteristics, controlling factors, and moisture sources of winter extreme precipitation events over South China could have great scientific as well as economic significance.

It is well known that extreme weather events are often caused by a combination of anomalous conditions in multiple atmospheric circulation systems (Li et al., 2019). Previous studies attributed the winter extreme precipitation events over South China to anomalies in the Western Pacific subtropical high, the East Asian major trough, the India-Burma trough, and the formation of the European blocking high (Wang et al., 2000; Zong et al., 2014; Ding and Li, 2017; Huang et al., 2018b). In addition, the variation of winter precipitation was also found to be closely related to sea surface temperature over the Eastern Tropical Indian Ocean and the South China Sea (Zhou et al., 2010; Li et al., 2015a). In addition to dynamic and thermal conditions, abundant moisture supply is also an essential condition for winter extreme precipitation events (Yang et al., 2019; Zhao et al., 2021). Therefore, exploring the moisture sources for the extreme precipitation events is a crucial part of understanding factors controlling these events. Previous climatological studies suggest that the most important moisture source regions for wintertime precipitation in South China were the South China Sea, western North Pacific, and the Bay of Bengal (Baker et al., 2015; Sun and Wang, 2015). However, detailed information about moisture transport and source regions of individual extreme precipitation events is largely lacking. Moreover, the large-scale atmospheric circulation patterns are not changing significantly at short time scale, so it is difficult for climatological studies to capture the possible rapid switching of moisture sources during an extreme precipitation event.

Stable isotopes in precipitation and water vapor ($\delta^{18}O$ and δ^2H) are useful natural tracers for the hydrological cycle (Araguás-Araguás et al., 2000; Galewsky et al., 2016). They have been used to trace moisture sources (Bonne et al., 2014; He et al., 2016) and identify water vapor transport pathways (Tian et al., 2007; Cai and Tian, 2016). Earlier studies have improved our understanding of the variations of stable isotopic compositions at different time scales, especially at the

2

monthly and daily scales. The variability of stable isotopic compositions is not only affected by local meteorological factors, such as temperature and precipitation amount (Dansgaard, 1964; Yu et al., 2015), but also by large-scale atmospheric circulations (Zhou and Li, 2017; Gao et al., 2018), and sources of moisture (Peng et al., 2010; Wang et al., 2017). In addition, deuterium excess (d-excess), defined as d = δ^2H − 8 × δ^{18}O, is influenced by the evaporative and meteorological conditions in the moisture source region (Dansgaard, 1964; Merlivat and Jouzel, 1979), and often used as an indicator for changes in relative humidity at the source region or shifts in the moisture origin (Benetti et al., 2014). In addition to monthly and daily scales, precipitation and water vapor isotopes have also been used to study precipitation processes at the event scale. For instance, Tremoy et al. (2014) used high-frequency near-surface water vapor isotopic composition measurements to classify precipitation events in the Niamey region in Niger into three categories, and established the role of mesoscale subsidence and rain evaporation on the isotopic evolution. Li et al. (2015b) revealed the abundant water vapor supply from different moisture sources through continuous isotopic observation of a summer extreme precipitation event in Beijing. Han et al. (2020), based on a data set at 10-min sampling interval, showed that the rapid change of stable isotopes in precipitation is related to different moisture sources and transport paths in the marginal zone of East Asian monsoon. These studies demonstrated that high-resolution precipitation and/or water vapor isotopes observations are an effective tool to identify more detailed information about precipitation processes. However, precipitation and/or water vapor isotopes observation during an extreme precipitation event is sparse, which limits our ability to study extreme precipitation processes by water isotopes. Existing studies on precipitation and water vapor isotopes often used monthly and daily data, which do not have the temporal resolution needed to study isotopic changes during individual precipitation events. In addition, continuous collection of precipitation isotope data through precipitation events is often difficult due to adverse weather conditions. Therefore, a continuous monitoring of water vapor isotopes at high temporal resolution (from minutely to hourly timescales) provides a feasible way to identify changes in the moisture sources during precipitation events. Moreover, compared with precipitation, water vapor responds more sensitively to changes in atmospheric circulation (Yao et al., 2018; Li et al., 2020b).

From December 2018 to February 2019, the joint influence of the central Pacific El Niño and East Asian Winter Monsoon quasi-biweekly oscillation led to a long period of persistent rainfall in Southeast China. The 51 accumulated rainy

3

days had the highest regional effective precipitation since 1981 (Guo et al., 2019; Wang et al., 2020). The regional sunshine duration was only half of the normal condition with the lowest number of sunshine hours recorded since 1961 (Li et al., 2020c). This record-breaking event provided an opportunity for using stable isotopes to understand the possible causes and moisture sources of winter extreme precipitation. In this study, we monitored and analyzed the stable isotopic compositions of water vapor (with hourly resolution) and precipitation (with daily resolution) during this extreme precipitation period in Nanjing, Southeast China. We utilized these high temporal resolution data to investigate the evolution of the stable isotopic compositions in water vapor during this period, and understand how event-scale isotopic variation is affected by climate factors and moisture sources during winter extreme precipitation events.

2 Materials and methods

2.1 Study site

Sampling and measurement of stable isotopes in water vapor and precipitation were carried out at the Station for Observing Regional Processes of the Earth System of Nanjing University (SORPES-NJU, 32.12°N, 118.95°E, 55 m a.s.l.above sea level) on the Xianlin Campus of the Nanjing University, about 20 km east of downtown Nanjing in Southeast China (Li et al., 2020b).

Nanjing is located in the lower reaches of the Yangtze River in China and has a typical subtropical monsoon climate. Under the influence of the East Asia Monsoon, it has a strongly seasonal climate with hot and rainy summers and cold and dry winters. In the winter (December–February, DJF), Nanjing is under the influence of the East Asian Winter Monsoon. According to the historical meteorological data (1981–2010), the average DJF monthly precipitation is 42 mm. From December 2018 to February 2019, affected by the continuous rainy weather, Nanjing has 46 accumulated rainy days and the total accumulated precipitation is 259 mm, more than double the seasonal average of 1981–2010 (Fig. 1).

2.2 Sampling and measurement

Water vapor sampling was carried out on the roof of the SORPES-NJU two-floor building from 1 November 2012 to the

4

present. Data from December 2018 to February 2019 was used for this study. The stable isotopic compositions of water vapor ($\delta^{18}O_v$ and δ^2H_v) were measured by a Picarro Wavelength Scanned Cavity Ring-Down Spectrometer (WS-CRDS, model: Picarro L2120–i). We calibrated the samples against various deviations (such as memory effect, drift effect, and concentration effect), following a set of procedures described in Gu et al., (2019) and Li et al., (2020b). We collected one sample every 2–3 seconds, and summarized the raw data into hourly averages for this study. The instrumental uncertainties were less than 0.2‰ for $\delta^{18}O_v$ and 1.0‰ for δ^2H_v (Gu et al., 2019).

Along with regular water vapor sampling, precipitation samples were collected on rainy days with an amount >0.1 mm from September 2011 to the present. Data from December 2018 to February 2019 was used for this study. All samples were poured into 100–ml polyethylene bottles immediately after collection. In order to avoid evaporation, all samples were refrigerated until being analyzed. The stable isotopic compositions in precipitation ($\delta^{18}O_p$ and δ^2H_p) were measured by a Picarro L2120–i in the Key Laboratory of Coast and Island Development of Ministry of Education, Nanjing University, China. The precision of measurements is 0.05‰ for $\delta^{18}O_p$ and 0.5‰ for δ^2H_p (Tang et al., 2015).

2.3 Trajectory weighted concentration field

In order to trace moisture source, we used the NOAA Hybrid Single Particle Lagrangian Integrated Trajectory (HYSPLIT) model and calculated backward trajectories of air masses associated with individual extreme precipitation events, using the Global Data Assimilation System (GDAS) with a spatial resolution of 1° × 1° as the background meteorological data (ftp://ftp.arl.noaa.gov/pub/archives/gdas1). Eight-day backward trajectories were calculated every one hour with the starting height of 1500 m above ground, because the average residence time of water vapor in the atmosphere is about 8 to 10 days (van der Ent and Tuinenburg, 2017).

Based on the HYSPLIT results, we calculated the Concentration Weighted Trajectory (CWT) field at 1° × 1°0.5° × 0.5° resolution to establish potential source regions that influence the isotopic variability of water vapor at the study site (Salamalikis et al., 2015; Bedaso and Wu, 2020; Li et al., 2020b). The CWT (C_{ij}) was calculated with the following equation:

$$C_{ij} = \frac{\sum_{k=1}^{K} C_k \tau_{ijk}}{\sum_{k=1}^{K} \tau_{ijk}} \ , \tag{1}$$

where (i, j) are grid indices, k is the trajectory index, K is the total number of trajectories that pass each $1° \times 1°$ ~~0.5° × 0.5°~~ grid, C_k the concentration (d-excess) measured upon arrival of trajectory k, and τ_{ijk} the residence time of trajectory k in grid cell (i, j).

2.4 Meteorological and reanalysis data

We obtained long-term monthly mean (1981–2010) and hourly meteorological data (air temperature, precipitation amount, and relative humidity) from December 2018 to February 2019 at Nanjing meteorological station from China Meteorological Data Service Center. We also used reanalysis data, including relative humidity, specific humidity, temperature, and zonal and meridional wind components ~~We also used reanalysis data, including 850 hPa zonal and meridional wind components and temperature,~~ from the European Centre for Medium-Range Weather Forecasts (ECMWF) Copernicus Climate Data Store (https://cds.climate.copernicus.eu) and Global Precipitation Climatology Centre (GPCC) precipitation data from the NOAA Physical Sciences Laboratory (https://psl.noaa.gov/data/gridded/).

Unless explicitly noted, the anomalies for climate variables are calculated with respect to the average of 1981–2010.

2.5 Definition of the 2018/2019 winter extreme precipitation in Southeast China

In the 2018/2019 winter, the regional average cumulative effective precipitation days in Southeast China exceeded 51 days, breaking the historical record since 1981 (Guo et al., 2019). In Nanjing, where our research site is located, the seasonal average DJF precipitation of 1981–2010 is 126 mm. Accumulated precipitation is 259 mm in the 2018/2019 winter, more than double the seasonal average of 1981–2010 (Fig. 1). As a result, we defined the 2018/2019 winter as a typical long-term extreme precipitation period. Because some water vapor isotopic data at Nanjing were missing due to instrument repair or maintenance, five large-scale precipitation events were finally selected for analysis, including (a) December 4−11, (b) December 24−30, 2018, (c) January 7−11, (d) February 16−22, and (e) January 27−31, 2019.

3 Results

~~3.1 Variations of water vapor and precipitation isotopic compositions during precipitation events~~

Figure 2 shows the hourly average $\delta^{18}O_v$ and d_v, daily average of $\delta^{18}O_p$ and d_p, and hourly air temperature, relative humidity, ~~and~~ precipitation amount, and atmospheric stability for those five events. $\delta^{18}O_v$ varies from −23.6‰ to −12.4‰ (with an average of −18.1‰), and d_v ranges from 16.3‰ to 35.9‰ (with an average of 24.6‰). $\delta^{18}O_p$ has an range from −15.5‰ to −1.3‰ and an average of −7.0‰. d_p ranges from 13.5‰ to 32.5‰, with an average of 23.6‰. Stable isotopes in precipitation and water vapor have similar variation pattern. Therefore, only high temporal resolution water vapor isotope data are used for further analysis. Based on the large-scale atmospheric circulation patterns (Fig. 3), we group these precipitation events into three classes.

The first class (including event a and b) is defined as cold air mass dominated events. The beginning of the precipitation event was characterized by the southerly wind (Fig. 3a, b), the atmospheric stability was low (Fig. 2a, b) ~~and higher temperature (Fig. 2a, b)~~. With the invasion of the cold air mass through the majority of the event period, the study site experienced northerly wind and temperature decrease, the atmospheric stability was gradually increasing (Fig. 2a, b). Towards the end of the event, the site returned to southerly wind with temperature increase, and the atmospheric stability decreased. Under this circulation background, the $\delta^{18}O_v$ value was generally high at the beginning, decreased significantly during the events, and gradually increased again toward the end of the events, whereas the d_v value showed the opposite trends (Fig. 2a, b). ~~The lowest $\delta^{18}O_v$ and highest d_v values were usually observed at the lowest temperature and relative humidity. However, changes in temperature and relative humidity cannot completely explain the variation in the $\delta^{18}O_v$ and d_v values. Air temperature and relative humidity data obtained from the meteorological station only reflect the local conditions at the sampling site (He et al., 2018), and the large-scale atmospheric circulation plays a more important role.~~

The second class (event c and d) is defined as warm air mass dominated events. Northerly wind and low temperature occurred only at the beginning of the precipitation event, whereas the majority of the even period was characterized by southerly wind and warm temperature (Fig. 3c, d). The atmospheric stability was relatively high at the beginning but soon decreased and remained low throughout the events (Fig. 2c, d). Similar to the first class, the $\delta^{18}O_v$ value was generally high

at the beginning, decreased significantly during the events, and gradually increased again toward the end of the events (Fig. 2c). However, different from the first class, <u>both $\delta^{18}O_v$ and d_v values in this class showed changes in the same direction throughout the event</u>~~both $\delta^{18}O_v$ and dv values in this class showed many more fluctuations throughout the event~~ (Fig. 2c, d). ~~The lowest $\delta^{18}O_v$ and d_v values occurred at the lowest temperature and highest relative humidity, it is significantly different from the first class.~~

In addition to the above two classes, the third class (event e) is characterized by alternating cold and warm air masses. The event started with northerly wind and low temperature, followed by southerly wind and temperature increase, and ended with northerly wind and temperature decrease (Fig. 3e). <u>The atmospheric stability was relatively high at the beginning, gradually decreased, and then increased in the later stage (Fig. 2e).</u> The $\delta^{18}O_v$ value remained constant in the early stage until it decreased suddenly at the end, whereas the d_v value showed great fluctuations (Fig. 2e).

~~**3.2 Intra-event variation of water vapor isotopic compositions**~~

~~Significant variations in $\delta^{18}O_v$ and d_v values of water vapor are observed within each event. We used the concentrated rainfall period of each event and divided it into different stages (Fig. 2), based on the above three classifications and the temporal patterns of variation in water vapor $\delta^{18}O_v$ and d_v.~~

~~The first class (Fig. 2a, b) of the precipitation events can be divided into four stages. (In the last stage of event b was not delineated because of missing data.) In stages 1 and 2, the $\delta^{18}O_v$ values continued to decrease, which was consistent with the temperature effect (i.e. stable isotopes had a significant positive correlation with air temperature). The d_v value first decreased (or remained stable), then increased, suggesting a gradual shift of water vapor source from ocean to land (Fig. 2a, b). Generally, atmospheric water vapor from the dry and cold regions shows a more negative $\delta^{18}O$ value and relatively high d-excess value (Uemura et al., 2008; Kostrova et al., 2020). In stage 3, the $\delta^{18}O_v$ and d_v value fluctuated without any obvious trends as a whole, mainly due to the mixing of oceanic and inland water vapor. In stage 4, the $\delta^{18}O_v$ value continued to decline, consistent with the rainout effect (i.e. stable isotopes continued to decrease with the increase of precipitation amount); the d_v value was significantly lower than the stage 3 with no obvious trend, reflecting the stable influence of oceanic water vapor (Fig. 2a).~~

8

~~The second class (Fig. 2c, d) of the precipitation events can be divided into three stages. In stage 1, the $\delta^{18}O_v$ value continued to decrease, consistent with the rainout effect; the d_v value continued to decrease, suggesting a shift of water vapor source from land to ocean. In stage 2, both the $\delta^{18}O_v$ value and d_v values increased, but still lower than the initial value in stage 1, suggesting increasing contribution of local inland water vapor in the mixture of oceanic and inland water vapor. In stage 3, the $\delta^{18}O_v$ value and d_v values showed a downward trend, reflecting the continuous influence of oceanic water vapor.~~

~~The third class (Fig. 2e) of the precipitation event can be divided into two stages. The $\delta^{18}O_v$ value was stable and relatively high in stage 1, possibly due to the influence of local inland water vapor in South China, where the air temperature remained high, leading to enriched isotopic values. The $\delta^{18}O_v$ value started to decline in stage 2, likely caused by the rainout effect. The d_v value is relatively high in stage 1, likely due the contribution of local inland water vapor. The rapid decrease of dv in the middle may indicate the influence of oceanic water vapor. In stage 2, the d_v value decreases rapidly, reflecting the rapid change of moisture sources, and a shift from mixed water vapor to oceanic water vapor.~~

4 Discussion

4.1 Controlling factors for water vapor isotopic variations during precipitation events

Significant variations of $\delta^{18}O_v$ and d_v in water vapor are observed within each event. In order to explore the controlling factors for the isotopic variations, we divided the concentrated rainfall period of each event into different stages (Fig. 2) based on temporal variation patterns of $\delta^{18}O_v$ and d_v.

The first class (Fig. 2a, b) of the precipitation events can be divided into four stages (the last stage of event b is not delineated because of missing data). In stages 1 and 2, the $\delta^{18}O_v$ value continued to decrease with decreasing temperature due to the temperature effect, i.e., the isotopic composition has a significant positive correlation with air temperature. The d_v value first decreased (or remained stable), and then increased, suggesting a gradual shift of water vapor source from ocean to land (Fig. 2a, b). Generally, atmospheric water vapor from the dry and cold regions shows a more negative $\delta^{18}O$ value and relatively high d-excess value (Uemura et al., 2008; Kostrova et al., 2020). In stage 3, the $\delta^{18}O_v$ and d_v values fluctuated without any obvious trends as a whole, mainly due to the mixing of oceanic and inland water vapor. In stage 4, the $\delta^{18}O_v$

9

value continued to decline due to the rainout effect of precipitation. Lower atmospheric stability at the same time, suggests increasing convection, which tends to lower the stable isotopes in water vapor. The d_v value is lower in stage 4 than in stage 3 with no obvious trend, reflecting the stable influence of oceanic water vapor. The period in between precipitation (between stage 2 and stage 3) experienced the lowest $\delta^{18}O_v$ and highest d_v values with the lowest temperature and relative humidity (Fig. 2a, b), suggesting the dominant influence of the large-scale activity of cold air masses (Fig. 3a, b).

The second class (Fig. 2c, d) of the precipitation events can be divided into three stages. In stage 1, the $\delta^{18}O_v$ value continued to decrease due to the rainout effect of precipitation. The d_v value continued to decrease, suggesting a shift of water vapor source from land to ocean. In stage 2, both the $\delta^{18}O_v$ and d_v values increased, but still lower than the initial values in stage 1, suggesting increasing contribution of local inland water vapor in the mixture of oceanic and inland water vapor. In stage 3, the $\delta^{18}O_v$ showed a downward trend, and d_v showed a slight decrease, reflecting the continuous influence of oceanic water vapor. Previous studies indicated that raindrop re-evaporation could contribute to changes in isotopic composition in precipitation and water vapor (Laskar et al., 2014; Conroy et al., 2016; Tian et al., 2020; Li et al., 2021). Thus, we compared the observed water vapor isotopic ratios ($\delta^{18}O_v$) with the theoretical isotopic composition of the water vapor in equilibrium with that of the precipitation at local temperature ($\delta^{18}O_e$) during the five precipitation events (Fig. 4). The $\delta^{18}O_e$ values of the third and fourth precipitation days of event d are slightly larger than the observed water vapor $\delta^{18}O_v$ values, indicating the re-evaporation of falling raindrops. The relative fluctuations $\delta^{18}O_v$ and d_v (especially lower $\delta^{18}O_v$ in Fig. 2d) during stages 2 and 3 of event d may be caused by the effect of re-evaporation of precipitation.

The third class (Fig. 2e) of the precipitation event can be divided into two stages. The $\delta^{18}O_v$ value was relatively high with some fluctuations in stage 1, possibly due to the influence of local inland water vapor in South China, where the air temperature remained high (Fig. 2e), leading to enriched isotopic values. The $\delta^{18}O_v$ value started to decline in stage 2, likely caused by the rainout effect, reflecting the influence of increased convection (indicating the decrease of atmospheric stability) on the stable isotopes in water vapor. The d_v value was relatively high in stage 1, likely due to the main contribution of local inland water vapor. The rapid decrease of d_v in the middle may indicate the influence of oceanic water vapor. In stage 2, the d_v value decreased rapidly, reflecting the rapid change of moisture sources from land water vapor to oceanic water vapor.

The $\delta^{18}O_e$ values of the first and second precipitation days of event e are significantly greater than the observed water vapor $\delta^{18}O_v$ values (Fig. 4), also indicating the re-evaporation of falling raindrops. Thus, in addition to the alternating influence of inland and oceanic water vapor, the effect of re-evaporation of precipitation could also partly account for the relatively large fluctuations of $\delta^{18}O_v$ and d_v during stage 1.

4.~~1~~ 2 Moisture sources for five precipitation events

Previous studies demonstrated that seasonal variations in the stable isotopic compositions of precipitation are caused not only by local meteorological conditions (Dansgaard, 1964), but also by the different moisture sources (Bonne et al., 2020). The above analysis results show that the large-scale circulation patterns ~~(850 hPa meridional wind and temperature)~~ have an important influence on the event-scale stable isotopes in water vapor, and the variation of meridional wind often corresponds to the change of moisture source regions. Some studies indicated that the air masses could obtain specific isotopic signatures based on the meteorological conditions in the moisture source region before reaching a given sampling site (Salamalikis et al., 2015; Kostrova et al., 2020). Therefore, based on the CWT model, we calculated the d_v value concentration fields to investigate differences among moisture source regions and water vapor transport pathways.

As seen in Fig. 4~~5~~, we identified five major moisture source regions that affect the sampling site base on cluster analysis of backward trajectories during these precipitation events: South China, East China Sea, South China Sea, Bay of Bengal, and Continental regions (Northwest China and Mongolia). The air parcels passing areas indicated with warm colors exhibit high d-excess values in the sampling site ~~(Salamalikis et al., 2015)~~. Trajectories passing North China, Northwest China, and Mongolia correspond to higher d_v values in the sampling site (Fig. 4~~5~~), as they are associated with relatively dry and cold air masses from the inland region. Moisture from other sources show lower d_v values, due to higher relative humidity at the oceanic source regions (Fig. 4~~5~~). These results clearly indicate that the changes of moisture source regions could play an important role in the variation of water vapor isotopic compositions in winter extreme precipitation events. ~~Our observations are in good agreement with the observation of summer extreme precipitation event by Li et al., (2015b).~~ We believe that abundant moisture supply through multiple moisture sources is one of the necessary conditions for the 2018/2019 winter extreme precipitation events to last for a long time.

11

4.2 3 Rapid shift of moisture sources during a precipitation event

Fig. 2 shows the variation of stable isotopic values in different stages of the precipitation events divided by vertical blue dashed lines. From the above analysis, it can be seen that the intra-event variation of stable isotopic values in water vapor was mainly controlled by the change of moisture sources. Therefore, we believe that the turning points at the blue dashed lines reflected rapid shifts of moisture source regions. In order to verify this hypothesis, we plotted the relationship between the d_v value and 850 hPa wind direction in the study region. Figure 5 6 shows that variation of the d_v value is closely related to rapid change in the wind direction, especially near the turning point. For example, during event a (Fig. 5a6a), the d_v value was relatively low in the early stage, and the main wind directions are easterly and southeasterly, reflecting the influence of water vapor from the East China Sea. From the first vertical blue dashed line, the wind direction turned northerly. As a result, the d_v value gradually increased and remained high, mainly due to the influence of water vapor transported by cold air mass from Northwest China and Mongolia. In the later stage, the wind direction near the second vertical blue dashed line turned to southerly and southeasterly, and the d_v value decreased due to the water vapor from the East China Sea. Therefore, the high temporal resolution d_v value in water vapor can be used to identify the rapid shift of moisture source regions during the continuous extreme precipitation process. Our results are in good agreement with previous studies by Li et al. (2015b) and Han et al. (2020), who found that the moisture source and transport path can change rapidly during a precipitation event. In addition, the HYSPLIT trajectories before and after the turning points of d_v are significantly different (Figure not shown), providing further evidence that the turning points of d_v correspond to the rapid shift of moisture source regions.

5 Conclusions

In this study, we presented stable isotopes in atmospheric water vapor and precipitation for five extreme winter precipitation events in Nanjing, from December 2018 to February 2019. Our analyses suggest that the variations of water vapor isotope are largely influenced by the change of moisture sources. Based on the results of the CWT model, the sampling site received different proportions of water vapor from multiple sources throughout the study period, including South China, East China Sea, South China Sea, Bay of Bengal, and Continental regions (Northwest China and Mongolia). In particular, the turning

points of the water vapor d-excess during a precipitation event reflected the rapid shift of moisture source regions. Our results imply that multiple moisture sources and the rapid shift among them are important conditions for sustaining extreme precipitation events, especially in the relatively cold and dry winter.

Author contribution. Hongxi Pang and **Shugui Hou** conceived this study. Material preparation, data collection, and analysis were performed by **Tao Xu, Zhaojun Zhan,** and **Wangbin Zhang**. The first draft of the manuscript was written by **Tao Xu**. **All authors** contributed to a discussion of the results.

Competing interests. The authors declare that they have no conflicts of interest.

References

Araguás-Araguás, L., Froehlich, K., and Rozanski, K.: Deuterium and oxygen-18 isotope composition of precipitation and atmospheric moisture, Hydrol. Process., 14, 1341–1355, https://doi.org/10.1002/1099-1085(20000615)14:8<1341::AID-HYP983>3.0.CO;2-Z, 2000.

Baker, A., Sodemann, H., Baldini, J., Breitenbach, S., Johnson, K., Hunen, J. V., and Zhang, P. Z.: Seasonality of westerly moisture transport in the East Asian summer monsoon and its implications for interpreting precipitation $\delta^{18}O$, J.

300   Geophys. Res.-Atmos., 120, 5850–5862, https://doi.org/10.1002/2014JD022919, 2015.

Bedaso, Z. and Wu, S. Y.: Daily precipitation isotope variation in Midwestern United States: Implication for hydroclimate and moisture source, Sci. Total. Environ., 713, 136631, https://doi.org/10.1016/j.scitotenv.2020.136631, 2020.

Benetti, M., Reverdin, G., Pierre, C., Merlivat, L., Risi, C., Steen-Larsen, H. C., and Vimeux, F.: Deuterium excess in marine water vapor: Dependency on relative humidity and surface wind speed during evaporation, J. Geophys. Res.-Atmos.,

305   119, 584–593, https://doi.org/10.1002/2013JD020535, 2014.

Bonne, J. L., Masson-Delmotte, V., Cattani, O., Delmotte, M., and Steen-Larsen, H. C.: The isotopic composition of water vapour and precipitation in Ivittuut, southern Greenland, Atmos. Chem. Phys., 14, 4419–4439, https://doi.org/10.5194/acp-14-4419-2014, 2014.

Bonne, J. L., Meyer, H., Behrens, M., Boike, J., Kipfstuhl, S., Rabe, B., Schmidt, T., Schönicke, L., Steen-Larsen, H. C., and

310   Werner, M.: Moisture origin as a driver of temporal variabilities of the water vapour isotopic composition in the Lena River Delta, Siberia, Atmos. Chem. Phys., 20, 10493–10511, https://doi.org/10.5194/acp-20-10493-2020, 2020.

Cai, Z. and Tian, L.: Processes governing water vapor isotope composition in the Indo-Pacific region: Convection and water vapor transport, J. Climate., 29, 8535–8546, https://doi.org/10.1175/JCLI-D-16-0297.1, 2016.

Conroy, J. L., Noone, D., Cobb, K. M., Moerman, J. W., and Konecky, B. L.: Paired stable isotopologues in precipitation and

315   vapor: A case study of the amount effect within western tropical Pacific storms, J. Geophys. Res.-Atmos., 121, 3290–3303, https://doi.org/10.1002/2015jd023844, 2016.

Dansgaard, W.: Stable isotopes in precipitation, Tellus., 16, 436–468, https://doi.org/10.3402/tellusa.v16i4.8993, 1964.

Ding, F. and Li, C.: Subtropical westerly jet waveguide and winter persistent heavy rainfall in south China, J. Geophys. Res.-Atmos., 122, 7385–7400, https://doi.org/10.1002/2017JD026530, 2017.

320   Ding, Y., Wang, Z., Song, Y., and Zhang, J.: Causes of the unprecedented freezing disaster in January 2008 and its possible association with the global warming, Acta. Meteorol. Sin., 66, 808–825, 2008 (in Chinese with English abstract).

Gao, J., He, Y., Masson-Delmotte, V., and Yao, T.: ENSO effects on annual variations of summer precipitation stable isotopes in Lhasa, southern Tibetan Plateau, J. Climate., 31, 1173–1182, https://doi.org/10.1175/JCLI-D-16-0868.1, 2018.

14

Galewsky, J., Steen-Larsen, H. C., Field, R. D., Worden, J., Risi, C., and Schneider, M.: Stable isotopes in atmospheric water vapor and applications to the hydrologic cycle, Rev. Geophys., 54, 809–865, https://doi.org/10.1002/2015RG000512, 2016.

Gu, X., Pang, H., Li, Y., Zhang, W., and Wang, J.: Study on calibration method for atmospheric water vapor stable isotopes observed by cavity ring-down spectroscopy, Spectrosc. Spect. Anal., 39, 1700−1705, 2019.

Guo, L., Liu, B., and Zhu, C.: Extraordinary long wet spell in south of Yangtze River during 2018/2019 winter and its possible causes, Chinese. Sci. Bull., 64, 3498−3509, https://doi.org/10.1360/N972019-00357, 2019 (in Chinese with English abstract).

Han, T., Zhang, M., Wang, S., Qu, D., and Du, Q.: Sub-hourly variability of stable isotopes in precipitation in the marginal zone of East Asian monsoon, Water., 12, 2145, https://doi.org/10.3390/w12082145, 2020.

He, S. and Richards, K.: Stable isotopes in monsoon precipitation and water vapour in Nagqu, Tibet, and their implications for monsoon moisture, J Hydrol., 540, 615–622, https://doi.org/10.1016/j.jhydrol.2016.06.046, 2016.

He, S., Goodkin, N. F., Kurita, N., Wang, X., and Rubin, C. M.: Stable isotopes of precipitation during tropical Sumatra squalls in Singapore, J. Geophys. Res.‐Atmos., 123, 3812–3829, https://doi.org/10.1002/2017JD027829, 2018.

Huang, W., He, X., Yang, Z., Qiu, T., Wright, J. S., Wang, B., and Lin, D.: Moisture sources for wintertime extreme precipitation events over South China during 1979–2013, J. Geophys. Res.‐Atmos., 123, 6690–6712, https://doi.org/10.1029/2018JD028485, 2018a.

Huang, W., Yang, Z., He, X., Lin, D., Wang, B., Wright, J. S., Chen, R., Ma, W., and Li, F.: A possible mechanism for the occurrence of wintertime extreme precipitation events over South China, Clim. Dynam., 52, 2367–2384, https://doi.org/10.1007/s00382-018-4262-8, 2018b.

Kostrova, S. S., Meyer, H., Fernandoy, F., Werner, M., and Tarasov, P. E.: Moisture origin and stable isotope characteristics of precipitation in southeast Siberia, Hydrol. Process., 34, 51−67, https://doi.org/10.1002/hyp.13571, 2020.

Laskar, A., Huang, J., Hsu, S., Bhattacharya, S., Wang, C., and Liang, M.: Stable isotopic composition of near surface atmospheric water vapor and rain–vapor interaction in Taipei, Taiwan. J. Hydrol., 519, 2091–2100,

15

https://doi.org/10.1016/j.jhydrol.2014.10.017, 2014.

Li, X., Li, J., and Li, Y.: Recent winter precipitation increase in the Middle-Lower Yangtze River Valley since the Late 1970s:
A response to warming in the Tropical Indian Ocean, J. Climate., 28, 3857–3879,
https://doi.org/10.1175/JCLI-D-14-00701.1, 2015a.

Li, J., Tao, T., Pang, Z., Tan, M., Kong, Y., Duan, W., and Zhang, Y.: Identification of different moisture sources through
isotopic monitoring during a storm event, J. Hydrometeorl., 16, 1918–1927, https://doi.org/10.1175/JHM-D-15-0005.1,
2015b.

Li, C., Yang, H., and Zhao, J.: Combinational anomalies of atmospheric circulation system and occurrences of extreme
weather/climate events, Trans. Atmos. Sci., 42, 321–333, https://doi.org/10.13878/j.cnki.dqkxxb.20190302001, 2019 (in
Chinese with English abstract).

Li, X. and He, L.: Analysis of the February 2019 Atmospheric Circulation and Weather, Meteor. Mon., 45, 738–744, 2019 (in
Chinese with English abstract).

Li, X., Wang, C., Ling, T., Sun, C., Zhang, Y., and Wang, J.: Features and possible causes of the extreme precipitation
anomaly in China during winter 2019/2020, Front. Earth. Sci., 8, 596753, https://doi.org/10.3389/feart.2020.596753,
2020a.

Li, Y., An, W., Pang, H., Wu, S. Y., Tang, Y., Zhang, W., and Hou, S.: Variations of stable isotopic composition in
atmospheric water vapor and their controlling factors—A 6-Year continuous sampling study in Nanjing, Eastern China,
J. Geophys. Res.-Atmos., 125, e2019JD031697, https://doi.org/10.1029/2019JD031697, 2020b.

Li, X., Wen, Z., and Huang, W.: Modulation of South Asian Jet wave train on the extreme winter precipitation over Southeast
China: Comparison between 2015/16 and 2018/19, J. Climate., 33, 4065–4081,
https://doi.org/10.1175/JCLI-D-19-0678.1, 2020c.

Li, X., Tang, C., and Cui, J.: Intra-event isotopic changes in water vapor and precipitation in South China, Water., 13, 940.
https://doi.org/10.3390/w13070940, 2021.

Mercer, J. J., Liefert, D. T., and Williams, D. G.: Atmospheric vapour and precipitation are not in isotopic equilibrium in a

continental mountain environment, Hydrol. Process., 34, 3078–3101, https://doi.org/10.1002/hyp.13775, 2020.

Merlivat. L. and Jouzel. J.: Global climatic interpretation of the deuterium-oxygen 18 relationship for precipitation, J. Geophys. Res., 84, 5029–5033, https://doi.org/10.1029/JC084iC08p05029, 1979.

375   Peng, T. R., Wang, C. H., Huang, C. C., Fei, L. Y., Chen, C. T. A., and Hwong, J. L.: Stable isotopic characteristic of Taiwan's precipitation: A case study of western pacific monsoon region, Earth. Planet. Sc. Lett., 289, 357–366, https://doi.org/10.1016/j.epsl.2009.11.024, 2010.

Qin, P., Xie, Z., Zou, J., Liu, S., and Chen, S.: Future precipitation extremes in China under climate change and their physical quantification based on a regional climate model and CMIP5 model simulations, Adv. Atmos. Sci., 38,

380   460−479, https://doi.org/10.1007/s00376-020-0141-4, 2021.

Rahmstorf, S. and Coumou, D.: Increase of extreme events in a warming world, P. Natl. Acad. Sci. USA., 108, 17905−17909, https://doi.org/10.1073/pnas.1101766108, 2011.

Salamalikis, V., Argiriou, A. A., and Dotsika, E.: Stable isotopic composition of atmospheric water vapor in Patras, Greece: A concentration weighted trajectory approach, Atmos. Res., 152, 93−104, https://doi.org/10.1016/j.atmosres.2014.02.021,

385   2015.

Sun, B. and Wang, H.: Analysis of the major atmospheric moisture sources affecting three sub-regions of East China, Int. J. Climatol., 35, 2243–2257, https://doi.org/10.1002/joc.4145, 2015.

Tang, Y., Pang, H., Zhang, W., Li, Y., Wu, S., and Hou, S.: Effects of changes in moisture source and the upstream rainout on stable isotopes in precipitation—A case study in Nanjing, eastern China, Hydrol. Earth. Syst. Sci., 19, 4293−4306,

390   https://doi.org/10.5194/hess-19-4293-2015, 2015.

Tian, L., Yao, T., Macclune, K., White, J., Schilla, A., Vaughn, B., Vachon, R., and Ichiyanagi, K.: Stable isotopic variations in west China: A consideration of moisture sources, J. Geophys. Res.-Atmos., 112, D10112, https://doi.org/10.1029/2006JD007718, 2007.

Tian, L., Yu, W., Schuster, P. F., Wen, R., Cai, Z., Wang, D., Shao, L., Cui J., and Guo, X.: Control of seasonal water vapor

395   isotope variations at Lhasa, southern Tibetan Plateau, J Hydrol., 580, 1–11,

https://doi.org/10.1016/j.jhydrol.2019.124237, 2020.

Tremoy, G., Vimeux, F., Soumana, S., Souley, I., Risi, C., Favreau, G., and Oï, M.: Clustering mesoscale convective systems with laser-based water vapor $\delta^{18}O$ monitoring in Niamey (Niger), J. Geophys. Res.-Atmos., 119, 5079–5103, https://doi.org/10.1002/2013JD020968, 2014.

400 Uemura, R., Matsui, Y., Yoshimura, K., Motoyama, H., and Yoshida, N.: Evidence of deuterium excess in water vapor as an indicator of ocean surface conditions, J. Geophys. Res.-Atmos., 113, D19114, https://doi.org/10.1029/2008JD010209, 2008.

van der Ent, R. J. and Tuinenburg, O. A.: The residence time of water in the atmosphere revisited, Hydrol. Earth. Syst. Sci., 21, 779−790, https://doi.org/10.5194/hess-21-779-2017, 2017.

405 Wang, B., Wu, R. G., and Fu, X. H.: Pacific-East Asian teleconnection: How does ENSO affect East Asian climate? J. Climate., 13, 1517–1536, https://doi.org/10.1175/1520-0442(2000)013<1517:PEATHD>2.0.CO;2, 2000.

Wang, L. and Feng, J.: Two major modes of the wintertime precipitation over China, Chin. J. Atmos. Sci., 35, 1105–1116, https://doi.org/10.3878/j.issn.1006-9895.2011.06.10, 2011 (in Chinese with English abstract).

Wang, S., Zhang, M., Crawford, J., Hughes, C. E., Du, M., and Liu, X.: The effect of moisture source and synoptic

410 conditions on precipitation isotopes in arid central Asia, J. Geophys. Res.-Atmos., 122, 2667–2682, https://doi.org/10.1002/2015JD024626, 2017.

Wang, Z., Sun, J., Wu, J., Ning, F., and Chen, W.: Attribution of persistent precipitation in the Yangtze-Huaihe river basin during February 2019, Adv. Atmos. Sci., 37, 1389–1404, https://doi.org/10.1007/s00376-020-0107-6, 2020.

Xu, R., Zhang, T., Rao, X., and You, Y.: Analysis of the December 2018 Atmospheric Circulation and Weather, Meteor. Mon.,

415 45, 437–444, 2019 (in Chinese with English abstract).

Yang, Z., Huang, W., He, X., Wang, Y., Qiu, T., Wright, J. S., and Wang, B.: Synoptic conditions and moisture sources for extreme snowfall events over East China, J. Geophys. Res.-Atmos., 124, 601–623, https://doi.org/10.1029/2018JD029280, 2019.

Yao, T., Zhang, X., Guan, H., Zhou, H., Hua, M., and Wang, X.: Climatic and environmental controls on stable isotopes in

420   ~~atmospheric water vapor near the surface observed in Changsha, China, Atmos. Environ., 189, 252–263,~~
       ~~https://doi.org/10.1016/j.atmosenv.2018.07.008, 2018.~~

Yao, Y., Lin, H., and Wu, Q.: Subseasonal variability of precipitation in China during boreal winter, J. Climate., 28, 6548–
       6559, https://doi.org/10.1175/JCLI-D-15-0033.1, 2015.

Yu, W., Tian, L., Ma, Y., Xu, B., and Qu, D.: Simultaneous monitoring of stable oxygen isotope composition in water vapour
425   and precipitation over the central Tibetan Plateau, Atmos. Chem. Phys., 15, 10251–10262,
       https://doi.org/10.5194/acp-15-10251-2015, 2015.

~~Zhao, Y., Gui, H., Li, S., and You, Y.: Analysis of the January 2019 Atmospheric Circulation and Weather, Meteor. Mon., 45,~~
       ~~587–592, 2019 (in Chinese with English abstract).~~

Zhao, N., Manda, A., Guo, X., Kikuchi, K., Nasuno, T., Nakano, M., Zhang, Y., and Wang, B.: A Lagrangian view of
430   moisture transport related to the heavy rainfall of July 2020 in Japan: Importance of the moistening over the subtropical
       regions, Geophys. Res. Lett., 48, e2020GL091441, https://doi.org/10.1029/2020GL091441, 2021.

Zhou, B., Gu, L., Ding, Y., Shao, L., Wu, Z., Yang, X., Li, C., Li, Z., Wang, X., Cao, Y., Zeng, B., Yu, M., Wang, M., Wang,
       S., Sun, H., Duan, A., An, Y., Wang, X., and Kong, W.: The great 2008 Chinese ice storm: Its socioeconomic-ecological
       impact and sustainability lessons learned, B. Am. Meteorol. Soc., 92, 47–60, https://doi.org/10.1175/2010BAMS2857.1,
435   2011.

Zhou, J. and Li, T.: A tentative study of the relationship between annual $\delta^{18}O$ & δD variations of precipitation and
       atmospheric circulations—A case from Southwest China, Quatern. Int., 479, 117–127,
       https://doi.org/10.1016/j.quaint.2017.05.038, 2017.

Zhou, L., Tam, C. Y., Zhou, W., and Chan, J. C. L.: Influence of South China Sea SST and the ENSO on winter rainfall over
440   South China, Adv. Atmos. Sci., 27, 832–844, https://doi.org/10.1007/s00376-009-9102-7, 2010.

Zong, H., Bueh, C., Ji, L.: Wintertime extreme precipitation event over southern China and its typical circulation features.
       Chinese. Sci. Bull., 59, 1036–1044, https://doi.org/10.1007/s11434-014-0124-x, 2014.
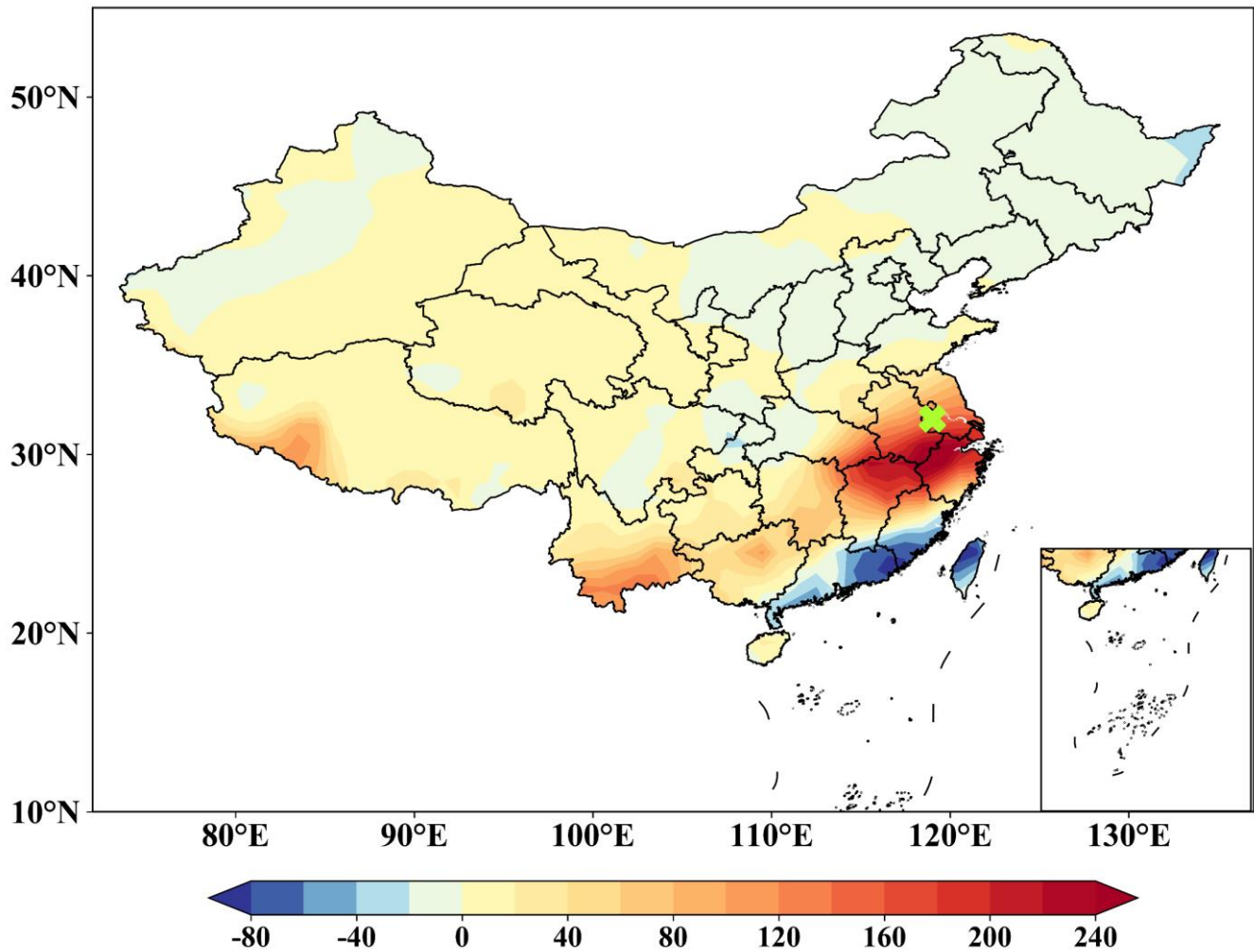
Fig 1. Winter (December–February) precipitation anomalies (shading; units: mm) over China in the winter of 2018/2019. "X"
represents the sampling site at Nanjing. The anomalies were calculated with respect to the 1981–2010 climatology (data from the
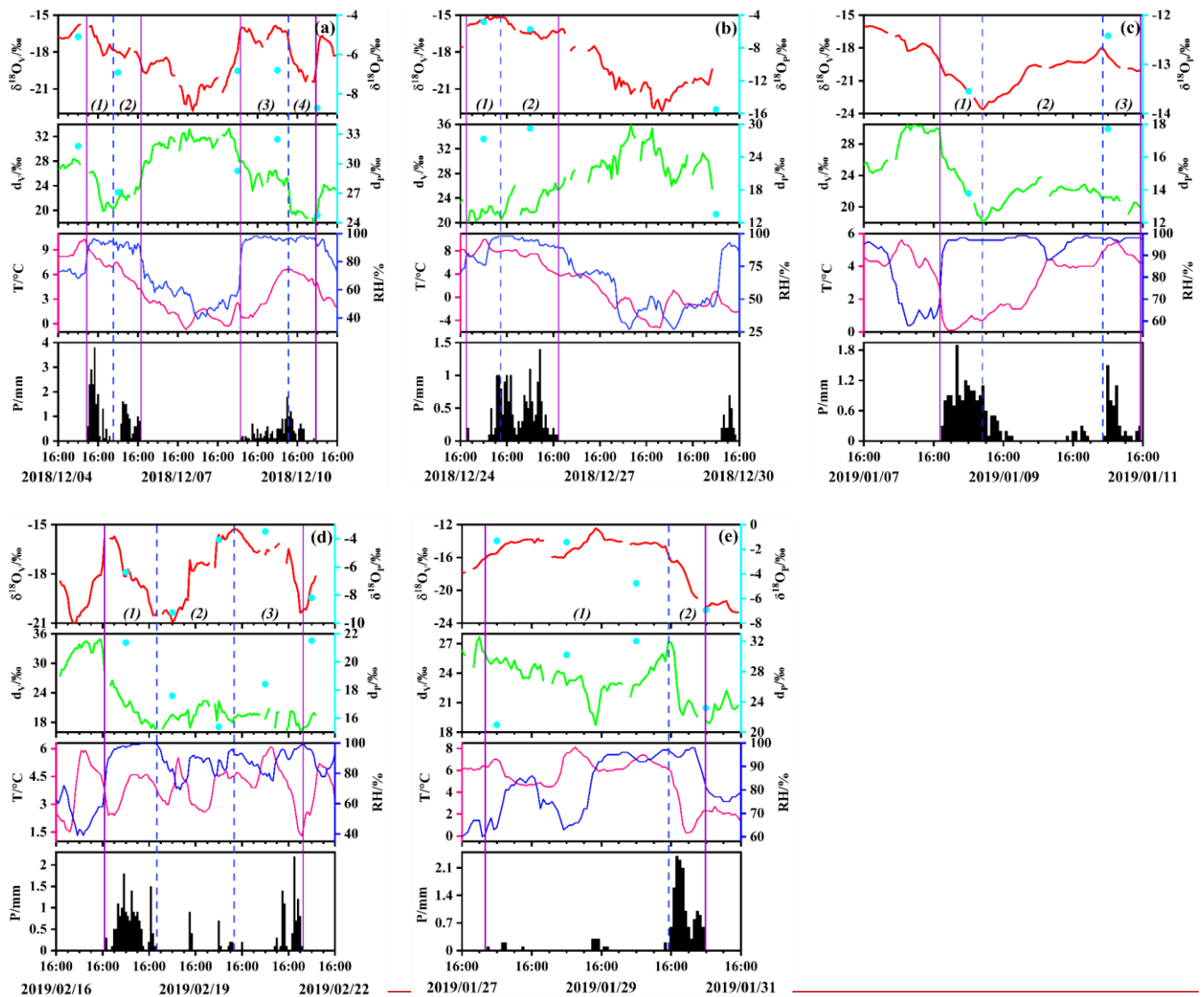**Global Precipitation Climatology Centre).**
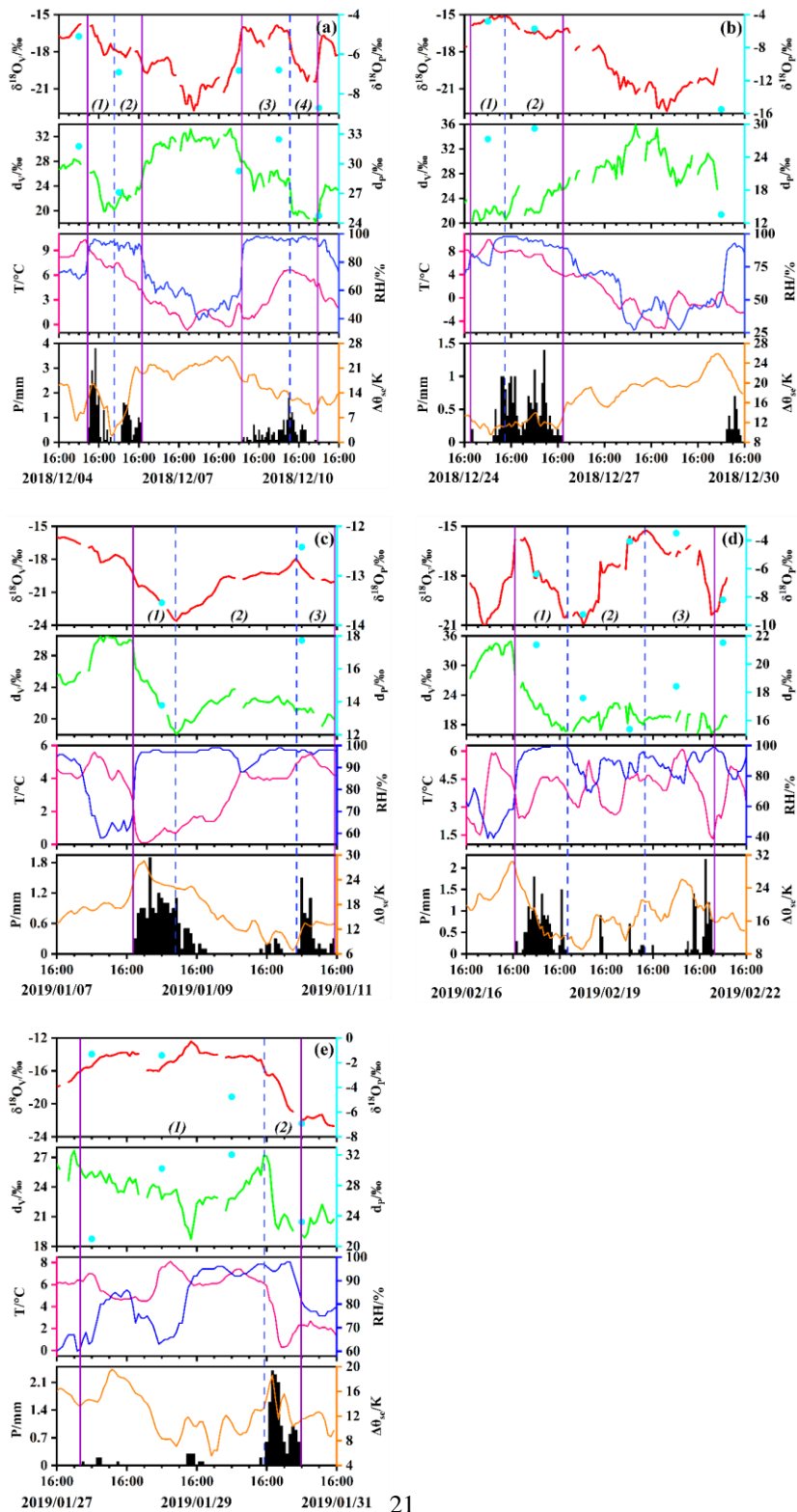
Fig 2. Time series of hourly water vapor $\delta^{18}O_v$ and d_v, daily precipitation $\delta^{18}O_p$ and d_p (cyan dots), air temperature (T), relative humidity (RH), ~~and~~ precipitation amount (P) , and atmospheric stability ($\Delta\theta_{se}$) at Nanjing. Atmospheric stability is the difference between the pseudo-equivalent potential temperature of 700 hPa and 850 hPa ($\Delta\theta_{se} = \theta_{se700} - \theta_{se850}$). (a) Event December 4−11, 2018; (b) Event December 24−30, 2018; (c) Event January 7−11, 2019; (d) Event February 16−22, 2019; (e) Event January 27−31, 2019. The vertical purple lines and blue dashed lines indicate the concentrated rainfall period and different stages of each precipitation event, respectively.
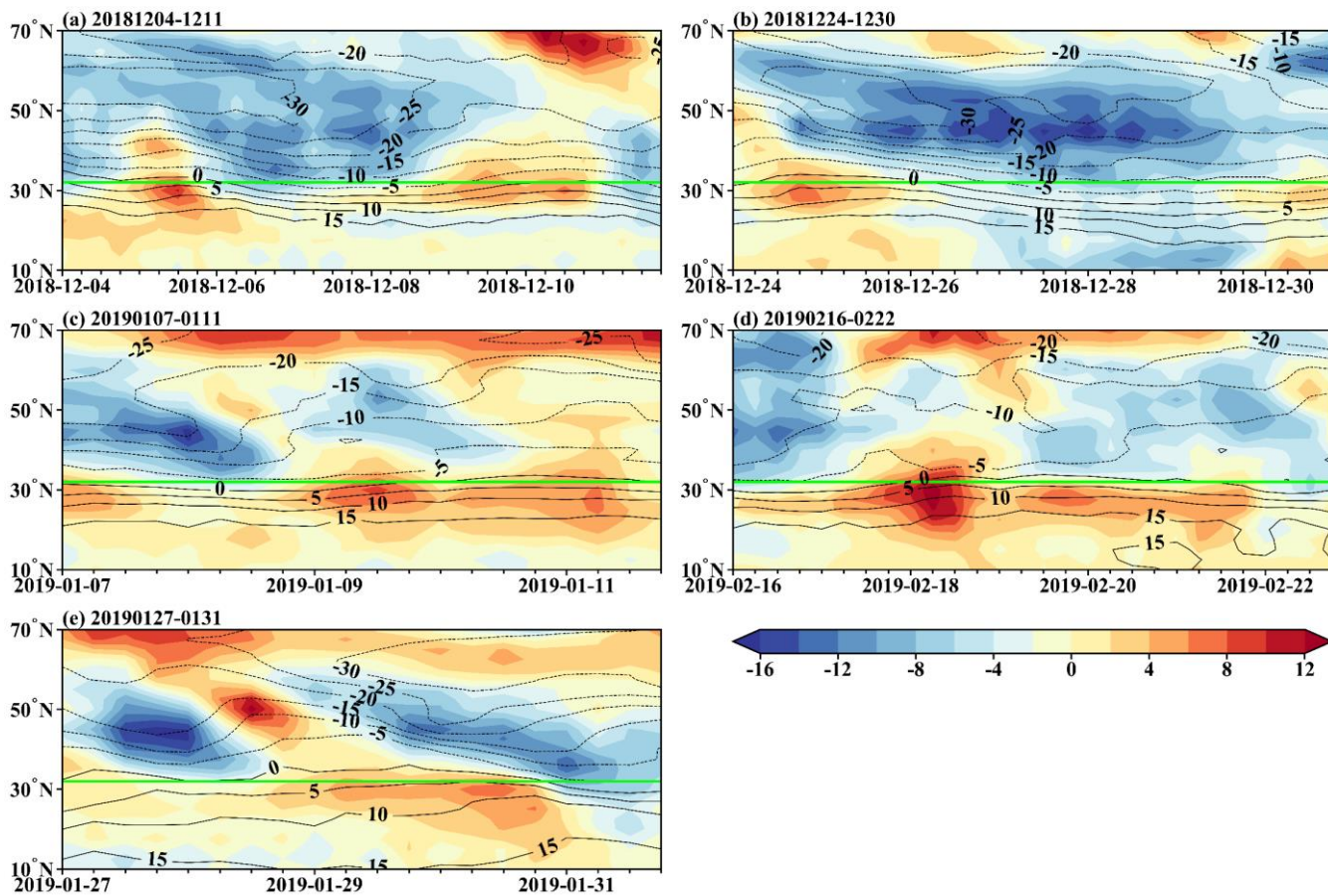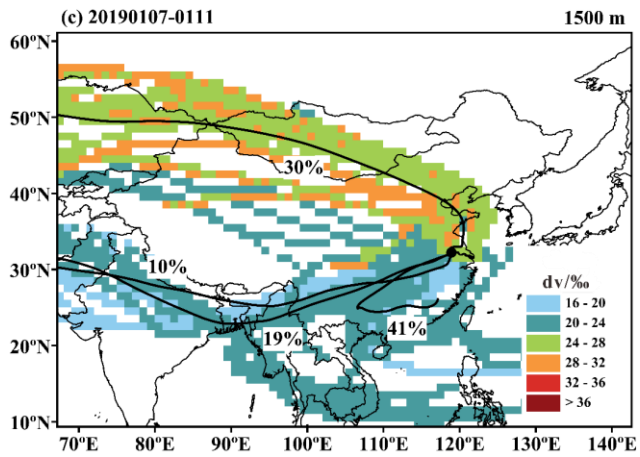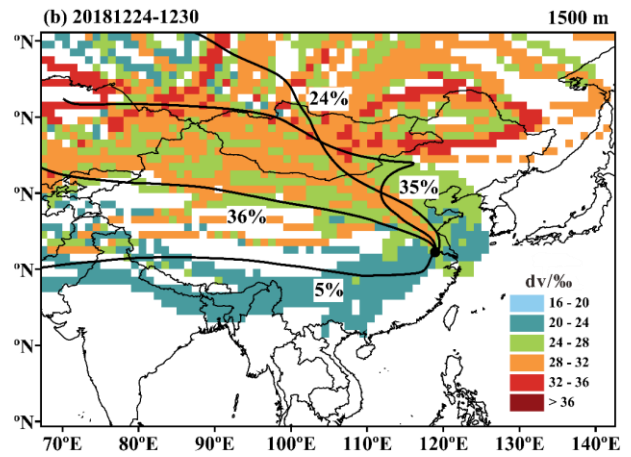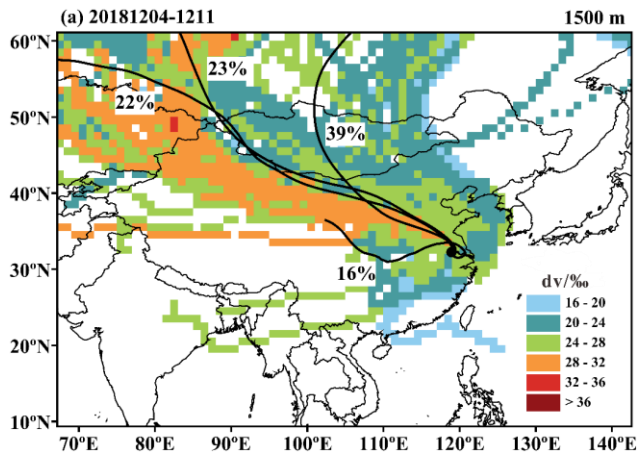
455

Fig 3. Latitude-time cross section of the meridional wind component (shading; units: m/s) and temperature (contour; units: °C) at 850 hPa along the 120°E. The horizontal green lines indicate the latitude of the sampling site at Nanjing (32.12°N).
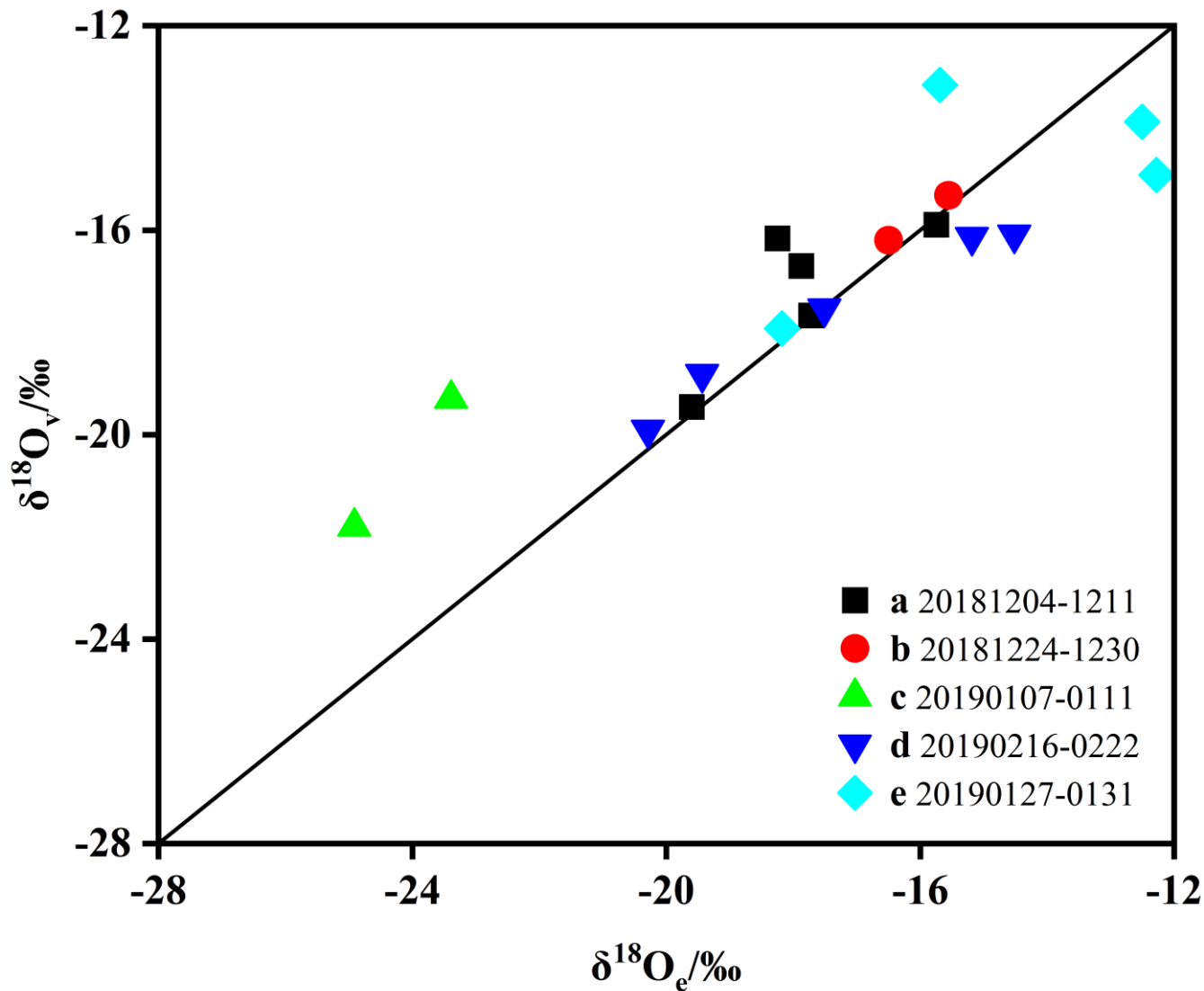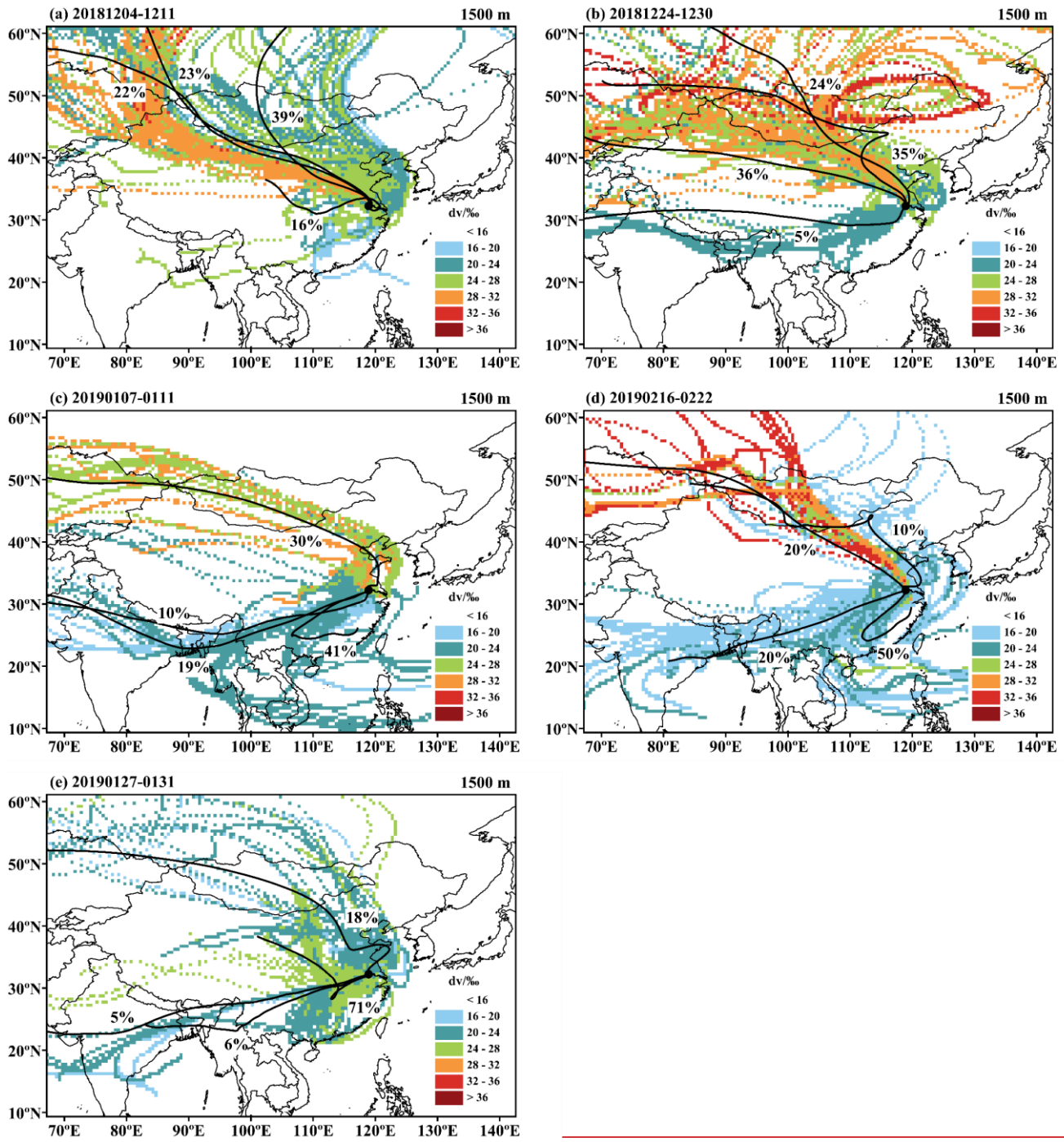
Fig 4. Relationship between observed ($\delta^{18}O_v$) and equilibrium ($\delta^{18}O_e$) vapor isotopic ratios in the five typical precipitation events. The isotopic composition of the water vapor theoretically in equilibrium with that of the precipitation ($\delta^{18}O_e$) is calculated by $\delta_e = (\delta_p - \varepsilon) / \alpha$, where ε is the equilibrium enrichment factor, and α is the liquid-to-vapor equilibrium fractionation factor (Mercer et al., 2020). The solid black line is the line of equilibrium.
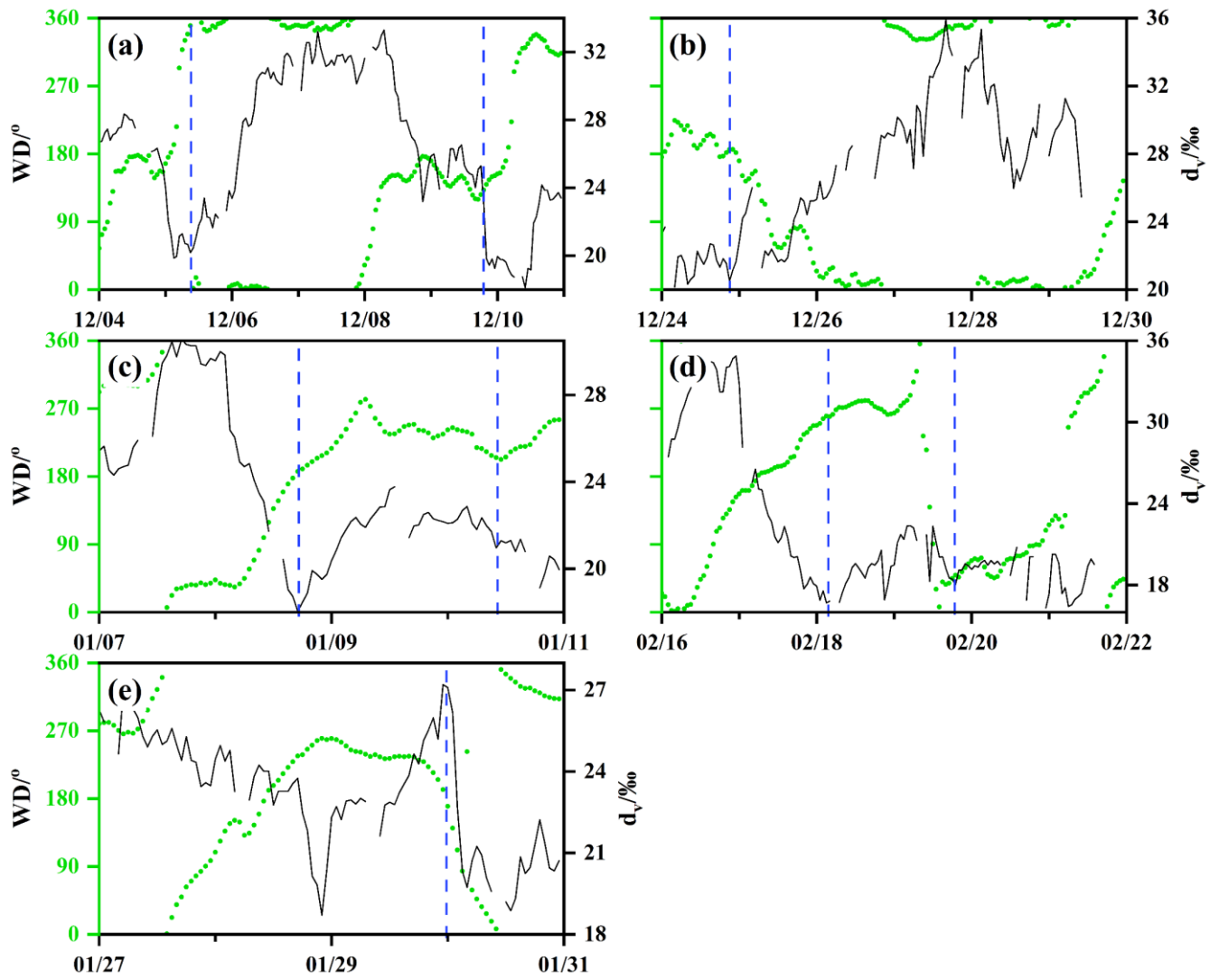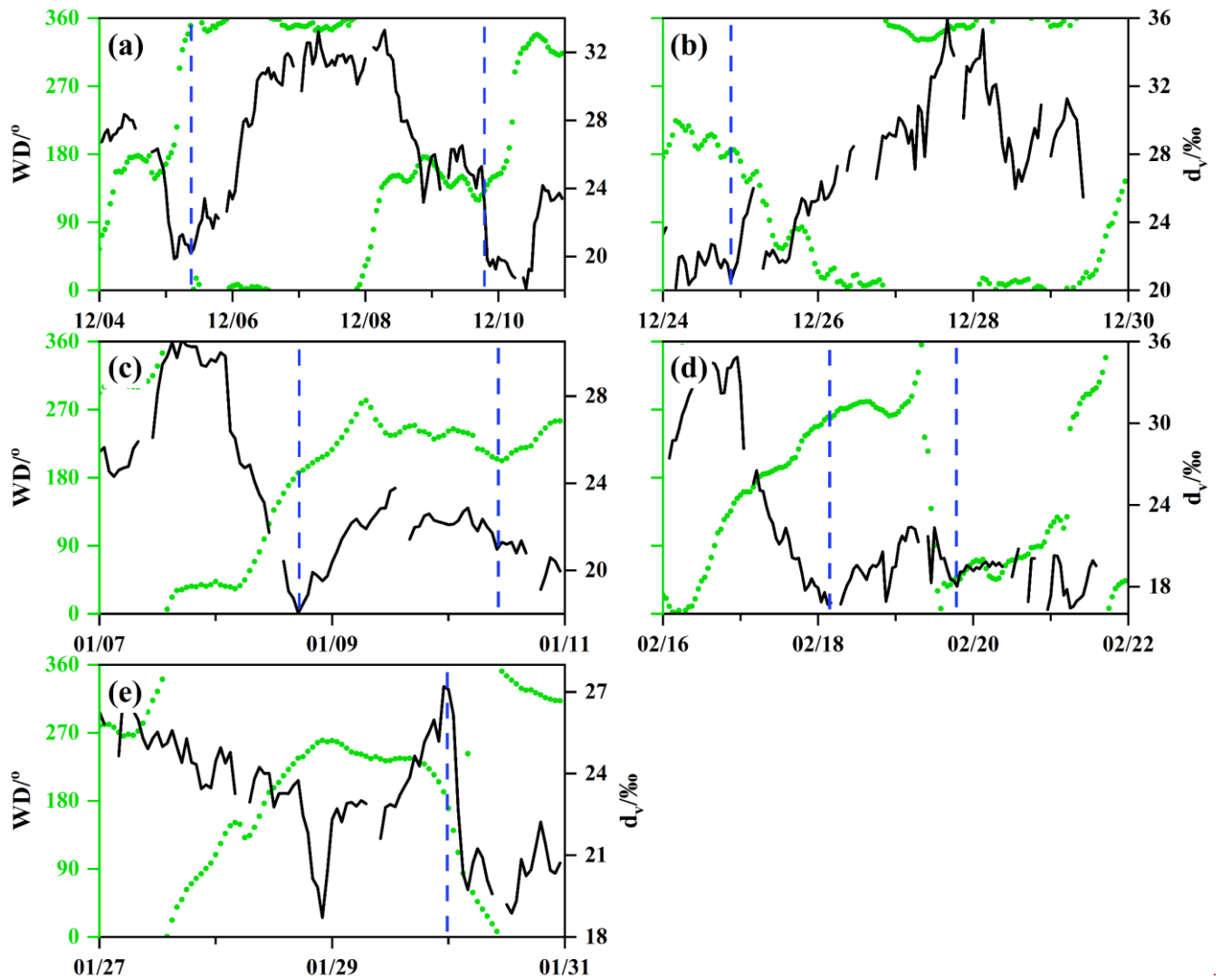
460

(a) 20181204-1211   1500 m
(b) 20181224-1230   1500 m
(c) 20190107-0111   1500 m
(d) 20190216-0222   1500 m
(e) 20190127-0131   1500 m
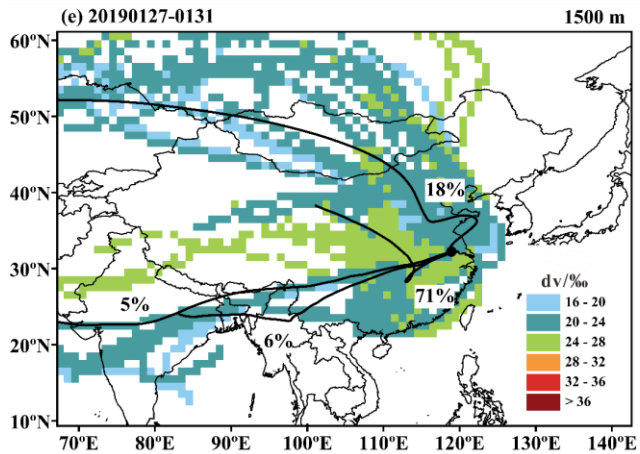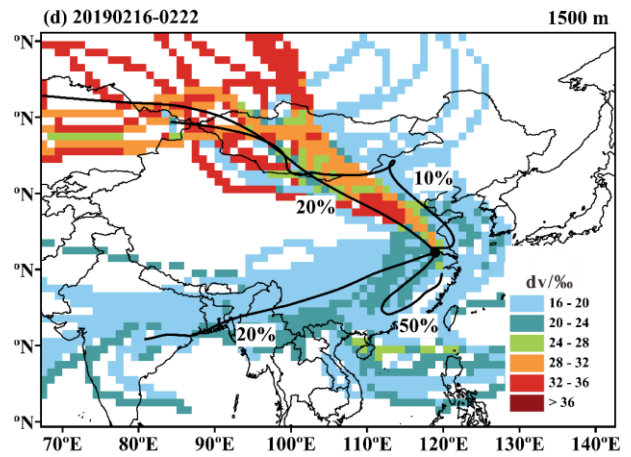
Fig 45. Concentration field of water vapor d_v for 192 h HYSPLIT back trajectories and clusters for the five typical precipitation events. The black circle indicates the location of Nanjing.

Fig 56. Time series of hourly water vapor d_v (black lines) and 850 hPa wind direction (green dots) of precipitation events. The vertical blue dashed lines indicate the different stages of precipitation events. (a) Event December 4−11, 2018; (b) Event December 24−30, 2018; (c) Event January 7−11, 2019; (d) Event February 16−22, 2019; (e) Event January 27−31, 2019.

470

28